Journal of Hazardous Materials 192 (2011) 1321–1329

Contents lists available at ScienceDirect

Journal of Hazardous Materials

journal homepage: www.elsevier.com/locate/jhazmat

Preparation and properties of silver nanoparticles loaded in activated carbon for biological and environmental applications

Tran Quoc Tuan[a], Nguyen Van Son[a], Hoang Thi Kim Dung[a], Nguyen Hoang Luong[a], Bui Thu Thuy[b], Nguyen Thi Van Anh[b], Nguyen Dinh Hoa[c], Nguyen Hoang Hai[a,*]

[a] Center for Materials Science, Hanoi University of Science, Vietnam National University, Hanoi, 334 Nguyen Trai, Thanh Xuan, Hanoi, Viet Nam
[b] Key Laboratory for Enzyme and Protein Technology, Hanoi University of Science, Vietnam National University, Hanoi, 334 Nguyen Trai, Thanh Xuan, Hanoi, Viet Nam
[c] Institute of Chemistry and Environment, 282 Lac Long Quan, Tay Ho, Hanoi, Viet Nam

ARTICLE INFO

Article history:
Received 23 March 2011
Received in revised form 25 May 2011
Accepted 15 June 2011
Available online 21 June 2011

Keywords:
Silver nanoparticles
Sonoelectrochemistry
Antibacterial materials
Activated carbon
Methylene blue

ABSTRACT

Silver nanoparticles colloid has been prepared by a modified sonoelectrodeposition technique in which a silver plate was used as the source of silver ions. This technique allows producing Ag nanoparticles with the size of 4–30 nm dispersed in a non-toxic solution. The Ag nanoparticles were loaded in a high surface activated carbon produced from coconut husk, a popular agricultural waste in Vietnam by thermal activation. The surface area of the best activated carbon is 890 m^2/g. The presence of Ag nanoparticles does not change significantly properties of the activated carbon in terms of morphology and methylene blue adsorption ability. The Ag nanoparticle-loaded activated carbon shows a good antibacterial activity against *Escherichia coli* with very low minimal inhibitory concentration of 16 μg/ml and strong As(V) adsorption. The materials are potential for prevention and treatment of microbial infection and contamination for environmental applications.

1. Introduction

General sanitation especially disease transmission via air or water is a serious problem in a developing country like Vietnam [1,2]. Hazards can be either physical, chemical, or microbiological agents of disease. Activated carbon, a product of popularly agricultural waste such as coconut husk [3], bamboo tree [4] is widely used for solving physical and chemical problems due to the fact that activated carbon (AC) possesses a large surface, so that high adsorption ability. However, to obtain a material which can solve not only physical, chemical but also microbiological problems as well is an interesting issue. Carbon materials are biocompatible with bacteria and good supports for their development [5]. An activated carbon material with antibacterial property can be obtained by impregnated with silver or metallic oxides. There are several ways to produce silver nanoparticles (AgNP) supported on activated carbon matrix. We applied a technique in which AgNP are directly loaded in AC. This is a simple way to produce a material with a highly antibacterial property [6].

Silver nanoparticles are commonly utilized nanomaterials due to their antibacterial properties, high electrical conductivity, and unique optical properties that could be used in various applications [7]. The interaction of light with metallic nanostructures excites plasmon resonance on their surfaces, which causes many interesting optical features [8]. At nanometer scale, AgNP have high surface area therefore they are highly reactive species. So that, silver has been a subject for many antibacterial applications [9,7]. It is believed that the high affinity of Ag towards sulfur or phosphorous is the key element of its antibacterial property. As sulfur and phosphorous are found in abundance throughout cell membrane, AgNP react with sulfur-containing proteins inside or outside the cell membrane, which in turn affects cell viability [10,11]. Another theory proposed that Ag^+ ions released from AgNP can interact with phosphorous moieties in DNA resulting in inactivation of DNA replication, or can react with sulfur-containing proteins to inhibit enzyme functions [12]. These properties allow the incorporation of AgNP into various matrix such as activated carbon, polymer networks, textiles, and wound dressing materials [13].

Many approaches have been developed to obtain AgNP of various shapes and sizes, including chemical reduction [14], laser ablation [15], gamma irradiation [16], electron irradiation [17], chemical reduction by inorganic and organic reducing agents [18], photochemical method [19], microwave processing [20], thermal decomposition of Ag oxalate in water and in ethylene glycol [21], and sonoelectrochemical method [22]. One of main disadvantages

* Corresponding author. Tel.: +84 4 3558 2216; fax: +84 4 3858 9496.
E-mail address: nhhai@vnu.edu.vn (N.H. Hai).

0304-3894/$ – see front matter © 2011 Elsevier B.V. All rights reserved.
doi:10.1016/j.jhazmat.2011.06.044

of those methods is the presence of unexpected toxic ions in the final products. The toxic ions in the product mostly are the ions of the silver precursor such as nitrate and thiolsulfate. A good silver precursor is silver acetate can be used [23]. But this chemical is expensive and the manipulation is difficult under ambient conditions.

Thus, this article reports a modified sonoelectrochemical technique to obtain AgNP in a non-toxic solution. The silver particles are then directly loaded on activated carbon produced by thermal activation of coconut husk. Testing on methylene blue (MB) adsorption of the activated carbon and the silver particle-loaded activated carbon shows that the presence of AgNP does not change the adsorption ability. In addition, AgNP brings an antibacterial property for the activated carbon and improves As(V) adsorption ability of AgAC.

2. Experimental

2.1. Preparation of silver nanoparticles

Silver nanoparticles have been prepared by a modified sonoelectrochemical method. The modification is that a silver plate was used as the cathode instead of silver salts to avoid unexpected ions from the salts. The cathode was made from a platinum plate. In a typical synthesis, the dimensions of both anode and cathode were 10 mm × 10 mm × 8 mm. A gap between the two electrodes was 5 mm. The electrolyte contained 600 mg of trisodium citrate (TSC) dissolved in 200 ml of doubly distilled water in a 250 ml beaker. The ultrasound emitter was a professional sonicator (Sonics VCX 750). The horn of the sonicator was placed at a position 2 cm far away from the cathode and the anode in the electrolyte, near the surface of the solution. The sonicator produced sonic pulses that immediately followed by current pulses. One pulse driver was used to control a galvanostat and the ultrasonic processor, which was adapted to work in pulsed mode. The ultrasound power was 200 W. The duration of the current pulse was 0.5 s then the current was turned off for a fixed duration of 0.5 s. When the current presented, Ag^+ ions were created from the anode and dissolved to the solution and AgNP were deposited on the surface of the electrode. Once the current was switched off, a 0.2 s ultrasonic pulse was used to dislodge the nanoparticles from the electrode. Total time of electrodeposition was 2 h. The current intensity was adjusted from 10 to 50 mA/cm^2. The concentration of TSC was changed from 0.5 to 4 g/l.

2.2. Preparation of activated carbon and silver-loaded activated carbon

A common agricultural residue-coconut husk was collected from the middle of Vietnam to make activated carbon by thermal activation [24]. The husk was washed and dried. Char was obtained by pyrolysis of the husk at 450 °C for 40 min. After being crushed and selected, 400 g of char with particle size of about 5 mm was loaded into a 300 ml stainless steel tube reactor. The tube was rotated at a rate of 4 rpm. A mixture of nitrogen and steam was passed through the char bed with the rate of 3 ml/min at 900 °C/1 atm for a period of time from 1 to 7 h. Activated carbon was obtained after removing ash by a solution 0.1 HCl and being dried at 100 °C. Ag nanoparticles (J = 50 mA/cm^2, c = 1.5 g/l) were loaded in AC (activation time of 5 h) by mixing AgNP solution with AC under vigorous stirring and ultrasound radiating for 1 h. The product of AgNP-loaded activated carbon (AgAC) powder was obtained by drying in air at 75 °C. The preparation factors were adjusted to have 1 wt.% of AgNP in AgAC. This AgAC was used in adsorption and antibacterial tests.

2.3. Adsorption experiments

The batch adsorption experiments of AC or AgAC were carried out in 250 ml Erlenmeyer flasks where 0.2 g of the AC or AgAC and 200 ml of methylene blue (MB) solutions (100–500 mg/l) were added and a magnetic stirring bar was placed in flask. The solutions were stirred at 120 rpm and 30 °C for 360 min to achieve equilibration. During the process, 2 ml of sample was taken and then centrifuged to remove AC or AgAC. The supernatant was subjected to measure the concentration of remained MB by studying the adsorption peak at 660 nm of the UV–vis spectra.

An As(V) solution was prepared by dissolving 1.0 mg of As_2O_5 into 1 l of doubly distilled water. The adsorption process was carried out by stirring 100 mg of AC or AgAC in 50 ml of arsenic solution for 3 h. Then adsorbent were collected by centrifugation. As(V) concentration in the remaining solution was determined by an atomic absorption spectroscopy.

2.4. Antibacterial experiments

We have conducted a qualitatively and a quantitatively antibacterial test. The antibacterial property of AgAC was examined by inhibition growth of *Escherichia coli* (*E. coli*) DH5α on Luria–Bertani (LB) agar 1.5% medium for the qualitative test whereas the antibacterial effect of AgNP was tested in LB broth (recipient: tryptone 10 g, yeast extract 5 g, NaCl 10 g, H_2O to 1 l) for the quantitative test.

For the qualitatively antibacterial assay of AgAC on LB agar medium, the composition of three Petri dishes was prepared as follows: only LB agar medium (disk (a)), LB agar medium mixed with 0.15 g AC (disk (b)), and 0.15 g AgAC (dish (c)). After solidification of the medium, *E. coli* was streaked uniformly on the three dishes and then incubated at 37 °C for 24 h. The growth of the bacteria was observed by white colonies appeared on the medium.

For the quantitatively antibacterial assay of AgNP in LB broth, the composition of 2 ml medium contained in several tubes was prepared as follows: only LB broth (negative control), LB broth supplemented with 120 μl TSC solution (TSC control), and LB broth supplemented with AgNP (AgNP antibacterial tests). The amount of AgNP was adjusted to have the concentration from 2 to 200 μg/ml. A single colony of *E. coli* DH5α was picked up and cultured overnight to grow until a concentration of 1.7×10^9 cells/ml (1 optical density at 595 nm, OD_{595}, equals to the concentration of 1.7×10^9 cells/ml). 1 μl of that overnight culture was transferred to those tubes so that the final concentration of *E. coli* DH5α obtained was 8.5×10^5 cells/ml. The tubes were then incubated in a shaker at 37 °C. Growth rate and bacteria concentration was determined by measuring the optical density at 595 nm OD_{595} after 4, 8, 24 and 30 h.

2.5. Equipments

The structure of materials was examined by X-ray diffractometer (XRD) D5005, Bruker, using Cu Kα radiation. Transmission electron microscope (TEM) measurements were carried out using a JEM-1200EX TEM instrument working at an accelerating voltage of 80 kV. AC and AgAC morphology was observed by using a Hitachi S-4700 field emission-scanning electron microscope (FE-SEM). Specific surface areas were measured by the Brunaur–Emmett–Teller (BET) method at 77 K using N_2 gas as an absorbent after heating the sample at 120 °C for 1 h. The chemical composition of the AgAC was studied by using an energy dispersion spectroscopy (EDS) in a JEOL 5410 LV scanning electron microscopy (SEM). UV–vis spectra of the samples were acquired in a UV-Vis

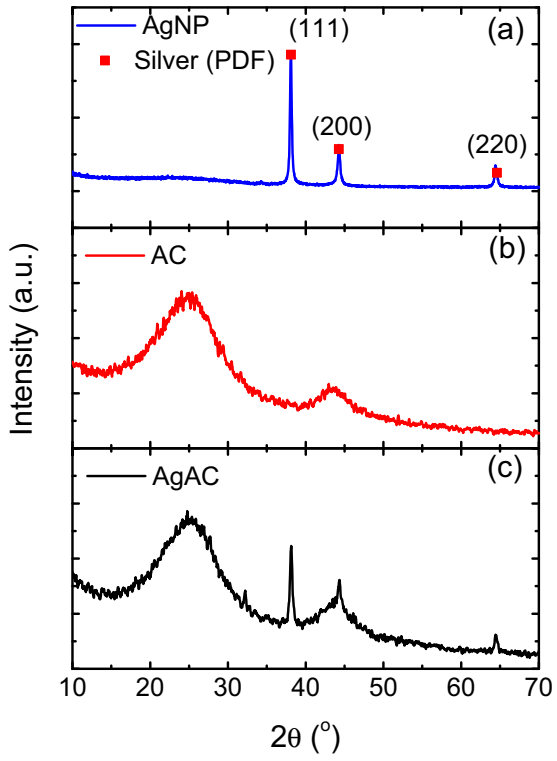

Fig. 1. XRD patterns of AgNP (a), AC (b) and AgAC (c). For silver preparation, the current intensity is 50 mA/cm^2; the TSC concentration is 1.5 g/l. The solid squares present for the powder diffraction file (PDF) of the fcc silver metal.

Specord 200 spectrophotometer (Analytik Jena, Germany) between 200 and 900 nm in a quartz cell of 5 mm path length. As(V) concentration was determined by a Shimadu AA-6800F atomic absorption spectroscopy (AAS). Centrifugation was carried out by a Hettich Universal 320, 9000 rpm, 20 min. Zeta potential was recorded by using a Zeta phoremeter IV-CAD Instrumentation at 40 °C.

3. Results and discussion

3.1. Structure, morphology and optical properties of AgNP, AC and AgAC

XRD patterns of the AgNP (J = 50 mA/cm^2, c = 1.5 g/l), AC (activation time of 5 h) and AgAC are shown in Fig. 1. The XRD patterns of AgNP show a face centered cubic structure presented by the diffraction peaks at 38.11°, 44.29° and 64.41°, which match well with the diffraction from the (1 1 1), (2 0 0) and (2 2 0) planes, respectively. From the full width at half-maximum (FWHM) of the (1 1 1) peak, a mean size of 23 ± 2 nm was estimated from the Scherrer formula: $d = 0.9\lambda/(\beta\cos\theta)$, where d is the mean size of particles, θ is the diffraction angle, β is the FWHM of the peak, and λ is the wavelength of the X-ray. Broad peaks of AC around 22° and 44° present for the amorphous nature of AC. The broad peaks of AC and the sharp peaks of silver appeared in the results of the AgAC display the coexistence of both AgNP and AC. The FWHM of the (1 1 1) peak of AgNP before and after being loaded onto AC are almost the same, which reveals that the size of AgNP did not change.

Morphology of AgNP can be controlled by many factors such as the current intensity, the concentration of TSC, the temperature of the electrolyte, the power of the ultrasonic waves, the area and distance between electrodes. In this study, we have fixed the area (1 cm^2), the distance (5 mm) between electrodes, the time of deposition (2 h), the preparation temperature (room temperature) and changed the concentration, c (g/l) of TSC and the current intensity, J (mA/cm^2) to obtain nanoparticles with different sizes. Fig. 2 presents the TEM images and size distribution of AgNP as a function of c and J. For the samples with J = 15 mA/cm^2, as the concentration of TSC increased from 0.5 g/l to 3.5 g/l, the mean size of particles d decreased from 12.8 nm to 4.0 nm and the size distribution varied from 4.8 nm to 1.2 nm (Table 1). TSC played a role as a conducting factor in the electrodeposition process. A high concentration of TSC should help the mass-transfer of silver ions in the electrolyte and, as the result, big particles would be expected. However, our results show that d was inversely proportional to c. This fact can be understood by the fact that TSC was not only a reduction agent but also a surfactant which supported particles dispersing in the solution. The $Ag^+ \rightarrow Ag^0$ reduction ability of TSC was high at about 90 °C however that ability was low at room temperature [25]. The temperature of the deposition was room temperature therefore the role of TSC in the preparation process is more a surfactant than a reduction agent. The surfactant molecules limits the growth of particles which resulted to small size when the concentration of TSC increased.

Table 1
The dependence of the particle size d and the size distribution σ on the current intensity J and the concentration of TSC c. Other preparation factors are fixed (see text for more detailed).

J (mA/cm^2)	c (g/l)	d (nm)	σ (nm)
15	0.5	12.8	4.8
15	1.5	6.0	2.6
15	3.5	4.0	1.2
30	1.5	18.9	7.5
50	1.5	22.9	9.8

We have fixed the TSC concentration of 1.5 g/l and changed J from 15 mA/cm^2 to 50 mA/cm^2 and the particle size correspondingly increased from 6.0 nm to 22.9 nm. The particle diameter of 22.9 nm corresponding to the preparation conditions J = 50 mA/cm^2, c = 1.5 g/l is close to that obtained from the XRD patterns (23 ± 2 nm). The particle size determined from the XRD data is the crystalline size whereas the size obtained from TEM is the morphological size. The fact that those two values are the same suggests that the silver particles were well crystallized. The formation rate of the silver at J = 50 mA/cm^2 was faster than that at J = 15 mA/cm^2. To obtain the same amount of silver particles, typically about 400 μg/ml, the preparation time was about 40 min in the former case where it was 120 min in the later case. Therefore we applied J = 50 mA/cm^2 and c = 1.5 g/l for making AgNP in later research, including the XRD results which is shown in Fig. 1. The dependence of the particle size on J can be understood by the fact that high current intensity fostered the mass-transfer of ions from the electrolyte to the cathode. For a same time of deposition, high current caused bigger particles and a higher formation rate than a low current did.

The UV–vis spectra of AgNP are presented in Fig. 3. There was an absorption band at around 400 nm which is ascribed to the surface plasmon absorption in metallic nanoparticles [26]. This value is commonly observed for AgNP prepared by other methods [17,27–29]. From Fig. 3, the surface plasmon resonance red-shifts with decreasing TSC concentration. As the particle size linearly reduced with the TSC concentration, the absorption peak moved to a longer wavelength with the particle size. The value of adsorption maximum, λ_{max} decreased almost linearly with increasing of the concentration of TSC from 406 nm for c = 4 g/l to 415 nm for c = 0.5 g/l. The dependence of the absorption peak on the size of nanoparticles when the size is very small compared to the wavelength of the incident light can be described by Mie theory for spherical objects [30–32]. Mie theory based on the Maxwell equation predicts a red-shift with increasing particle size.

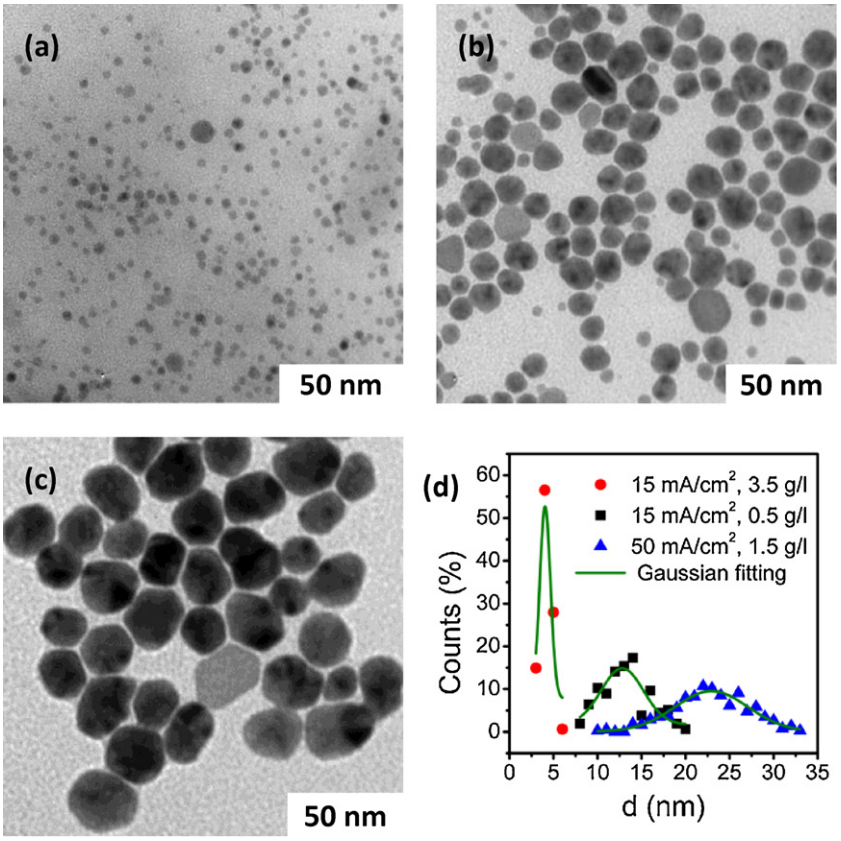

Fig. 2. TEM images of silver nanoparticles: $J = 15$ mA/cm^2, $c = 3.5$ g/l (a); $J = 15$ mA/cm^2, $c = 0.5$ g/l (b); $J = 50$ mA/cm^2, $c = 1.5$ g/l (c); and the corresponding size distributions of Ag nanoparticles (d).

SEM and TEM images of the carbon activated for 5 h are presented in Fig. 4(a) and (b). Activated carbon sample consists of many particles with random form and size. The size of AC particles varies from hundred of nm to few μm. There were many holes of few ten nm in the material. The existence of AgNP in AgAC sample may be recognized by the dark dots appeared in the TEM image (Fig. 4(c)) and the EDS spectra of this material (Fig. 4(d)). The average size of silver nanoparticles loaded to AC is 23 nm which is much bigger than the pore size of the activated carbon (about 1.8–2.2 nm) so that silver nanoparticles could not be loaded in those small pores. Instead, silver nanoparticles attached on the surface of AC or they can be loaded in bigger pores and spaces between particles.

The BET total surface area and pore volume depended on the activation time (Fig. 5(a)). Value of the BET surface area increased almost linearly with the activation time to a maximal value of 890 m^2/g for the sample annealed for 5 h and then declined at longer time. Similarly, the pore volume of AC got a maximal value of 0.45 cm^3/g for the sample with the activation time of 5 h. It required a period of time for material in the char being reacted completely but if the activation time was too long the fragile structure generated could block the pores inside the material. Therefore, the time of 5 h is optimal for the activation process. We use the carbon activated for 5 h for making AgAC and the MB adsorption studies and As(V) removal experiments.

Difference in adsorption–desorption isotherms from the BET results of carbon activated for 5 h and its AgNP-loaded material (Fig. 5(b)) is hardly recognized which confirms that the surface of AC did not changed with the presence of the AgNP. The BET surface area (890 m^2/g) of AC is almost the same as that of AgAC (880 m^2/g). The adsorption–desorption isotherms of the AC and AgAC shows

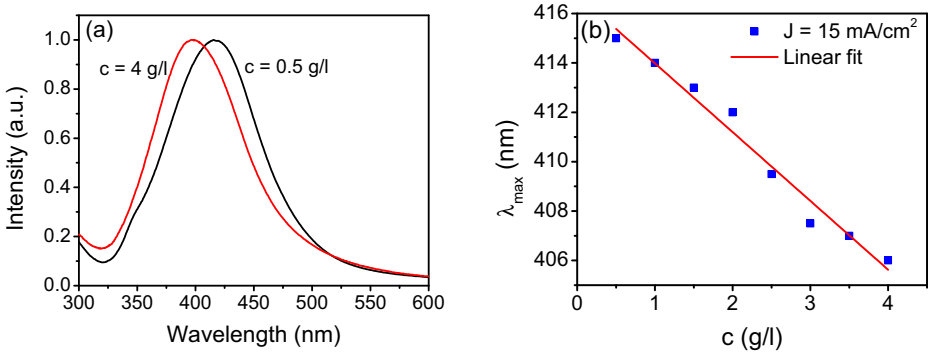

Fig. 3. UV–vis spectra of the silver nanoparticles produced by sonoelectrochemistry with $J = 15$ mA/cm^2 and $c = 0.5$ and 4.0 g/l (a) and the dependence of absorption maximum λ_{max} in the UV–vis spectra on the TSC concentration c (b).

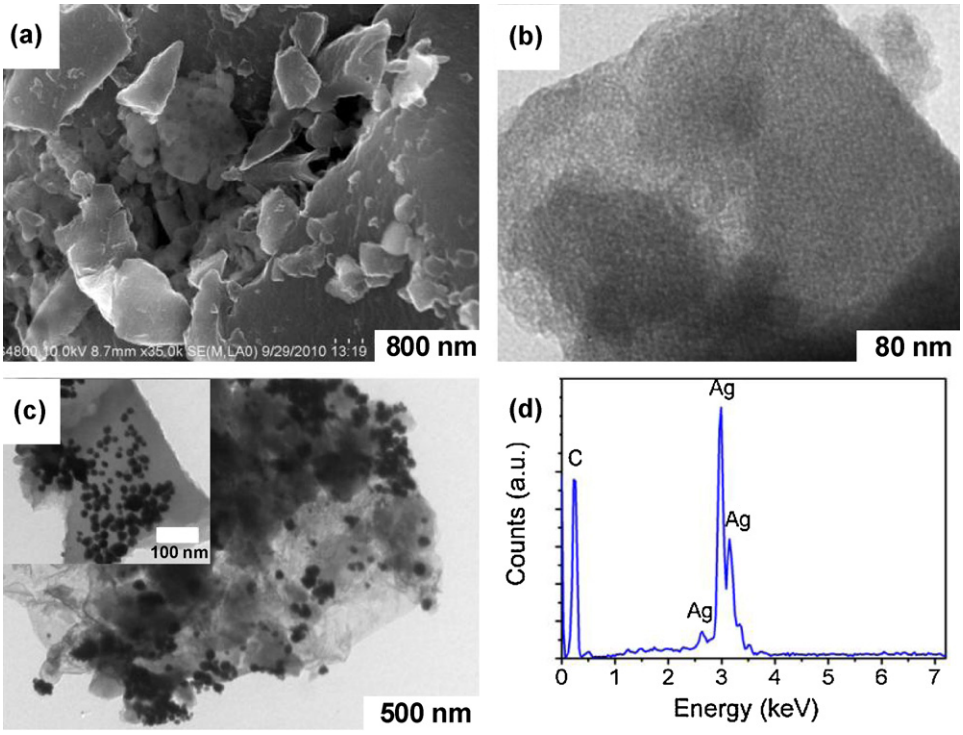

Fig. 4. SEM (a) and TEM (b) images of AC, TEM image of AgAC (c) and the EDS analysis on a part of AgAC (d).

that the hysteresis occurred at relative pressure $P/P_0 = 0.45$ which is slightly higher than the common value of 0.42 (the boiling point of nitrogen, independent of the nature of the porous adsorbent [33]). The higher closure point in AC between the adsorption and desorption branches may be due to the collapse of AC structure. This leads to pore blocking and eventually to the closure at higher pressures of nitrogen. The shape of the curve does not exhibit a limiting adsorption at relatively high pressure. This implies that the materials contain aggregates of platelike particles giving rise to narrow splitlike pores. We have observed a very similar behaviour for porous silicon in another study [34].

3.2. Adsorption study

Adsorption ability of the carbon activated for 5 h has been tested by studying MB adsorption. From UV–vis spectra, the intensity of the strongest adsorption peak at 660 nm was linearly proportional to the concentration of MB so that this peak was chosen to determine the concentration of MB in the solution. The amount of MB q (mg/g) adsorbed on a unit mass of AC depends on the initial concentration of MB c_0 (mg/l), the concentration of MB c (mg/l) at the time t, the volume of the solution v (l), the mass of the AC used m (g), as follows: $q = (c_0 - c)v/m$. The value of q and c is a function of time. As the time of interaction is large enough, the adsorption of MB molecules on AC surface balances with the desorption process – the equilibrium is formed and $q \to q_e$ and $c \to c_e$. The removal capacity at equilibrium state depends strongly on the surface area of AC, the pH of the solution, the temperature T, and the mechanism of the adsorption process. To elucidate the mechanism, study kinetic and isotherm models are required.

For the kinetic study, there are three kinetic models which are normally applied, which are pseudo-first-order [37], pseudo-second-order [38] and Elovich model [39]. The corresponding equations that describe those models respectively are:

$$q = q_e(1 - e^{-k_1 t}) \quad (1)$$

$$q = \frac{q_e^2 k_2 t}{1 + q_e k_2 t} \quad (2)$$

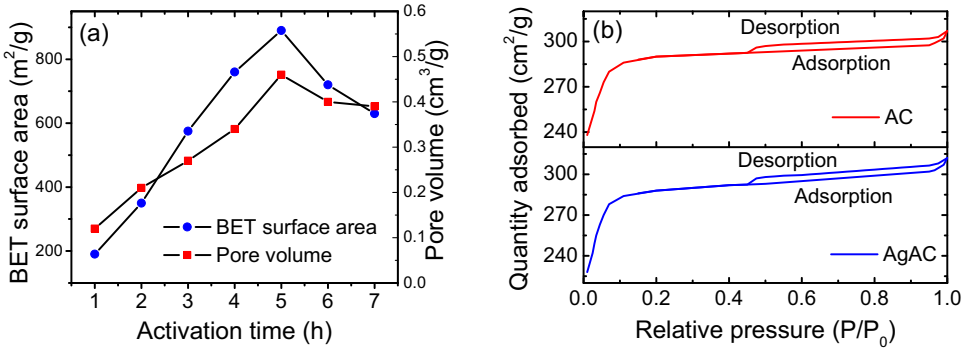

Fig. 5. The dependence of the total surface area and the pore volume determined from BET analysis on the activation time (a) and nitrogen adsorption–desorption isotherms for AC and AgAC with activation time of 5 h (b).

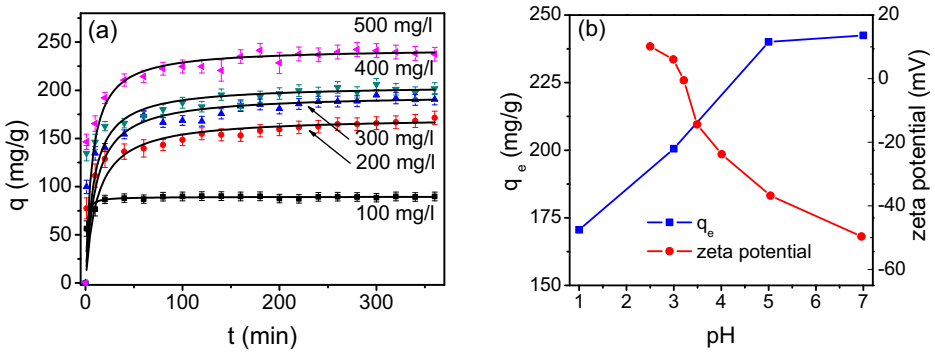

Fig. 6. Comparison between experimental data (dots) to the pseudo-second-order kinetics (solid curves) (a) and the dependence of methylene blue adsorption of the activated carbon and zeta potential on the solution pH (b).

$$q = \frac{\ln(1 + abt)}{b} \quad (3)$$

where k_1 is the rate constant of the pseudo-first-order adsorption, k_2 is the rate constant of the pseudo-second-order adsorption, a is the initial adsorption rate, and b is the desorption constant. Fitting the experimental data with those equations corresponding to the models reveals the mechanism of the adsorption process [40,41].

For the isotherm study, there are some isotherm models can be used but two models, i.e., the Langmuir and the Freundlich ones have been widely used. The Langmuir model which assumes that equilibrium is attained when a monolayer of the adsorbate molecules saturates the adsorbent [35]. The Freundlich model assumes heterogeneous surface energies, in which the energy term in the Langmuir equation varies as a function of the surface coverage [36]. The corresponding isotherm equations for those two models respectively are:

$$q_e = \frac{q_m k_a c_e}{1 + k_a c_e} \quad (4)$$

$$q_e = k_F (c_e)^{1/n} \quad (5)$$

where q_m is q_e for complete monolayer adsorption capacity; k_a is the equilibrium adsorption constant (l/mg); k_F is the Freundlich adsorption constant and $1/n$ is a measure of the adsorption intensity.

Fig. 6(a) shows the MB removal of AC as time changing. The conditions of these tests were the initial concentration c_0 = 100–500 mg MB/l, the amount of AC m = 0.2 g/200 ml, room temperature. All curves show an initial rapid development of adsorption which is due to large number of vacant sites available for adsorption at initial stages, so that, there existed an increased concentration gradient between adsorbate in solution and adsorbate in adsorbent [49,50]. In the first 20 min, about 70% of MB molecules were adsorbed. Later on, the number of available vacant sites reduced then the adsorption process reached the saturation process. The fittings with the three kinetic models show that the pseudo-second-order adsorption was the best model for describing adsorption mechanism of the AC (Fig. 6(a)). The correlation coefficients R^2 are higher than 0.998, the calculated q_e values are close to the experimental q_e values for all the cases (Table 2). Fittings with the other models are so poor with R^2 smaller than 0.8 (data not shown). Similar behaviour was observed for AC produced by other techniques [40,42,41]. The pseudo-second-order kinetic equation for adsorption is in line with the universal rate law for a chemical reaction [48]. Applying for our study, the rate of MB adsorption was determined by the availability of adsorption sites on the surface of AC rather than MB concentration. The ability for removing MB depends strongly on the surface property of AC. The presence of AgNP on AC may cause a change on its adsorption process. We have tested the MB adsorption property of AC and AgAC with the initial concentration c_0 = 200 mg MB/l and found no significant difference between the two materials. This is confirmed by the similarity of the BET isotherms of these two materials (Fig. 5(b)).

The pH of the solution is important for the adsorption process and particularly for the adsorption capacity. It is commonly known that at high pH values, cations are favourably adsorbed due to the negatively charged surface sites [47]. When dissolved in water, MB are cations because the MB molecules lose anions Cl^-. We expect an increase in adsorption capacity as increasing pH. It is shown in the dependence of MB adsorption on the solution pH of 1–7 with the initial MB concentration of 500 mg/l (Fig. 6(b)). The MB up-take q_e increased from 170 (at pH = 1)–240 mg/g (at pH = 5). Then q_e does not change significantly at higher pH. Zeta potential reveals that the surface charge of AC changed at pH = 3.2 (Fig. 6(b)). It means that at pH < 3.2, the surface charge of AC was positive which caused the low value of q_e. At pH > 3.2, the surface charge of AC was negative so that large number of MB molecules could be adsorbed on AC surface. The saturation of q_e at high pH depends on other factors such as surface area, adsorption mechanism and so on. This behaviour is commonly observed in MB [40] and malachite green [42] adsorption on AC.

Fig. 7(a) shows the comparison of the experimental data with two theoretical isotherm models at neutral pH. The fitting correlation coefficient R^2 deduced for the Langmuir and the Freudlich are 0.98 and 0.79, respectively. It is clear that the Langmuir model is suitable to describe the adsorption mechanism of AC than the Freundlich model. A value of 240 mg/g is obtained for the complete monolayer adsorption capacity q_m in the Langmuir model. The value of q_m is a high value compared to the range from few to about 200 mg/g in other reports [42–46].

The adsorption ability of AC and AgAC are different when the adsorbate is As(V). At equilibrium state, the As(V) adsorption ability of AC and AgAC was studied with same conditions of stirring time (3 h) and concentration of As(V) ions (1.0 mg/l). The results show that with 2 g of AC and AgAC per liter at neutral pH, the AC reduced the As(V) concentration by 5.5% while the AgAC reduced by 17.1%. There was an improvement in the reduce ability of As(V) ion concentration when the silver nanoparticles were loaded into AC. This behaviour has also been observed in studying of arsenate adsorp-

Table 2
Fitting parameters to the pseudo-second-order kinetic model.

c_0	$q_e^{exp.}$	$q_e^{cal.}$	k_2 ($\times 10^{-3}$)	R^2 ($\times 10^{-2}$)
100	89.8	89.4	2.4	100.0
200	171.5	174.8	0.4	99.8
300	190.6	198.4	0.4	99.9
400	201.8	207.5	0.4	99.8
500	237.5	245.1	0.5	99.9

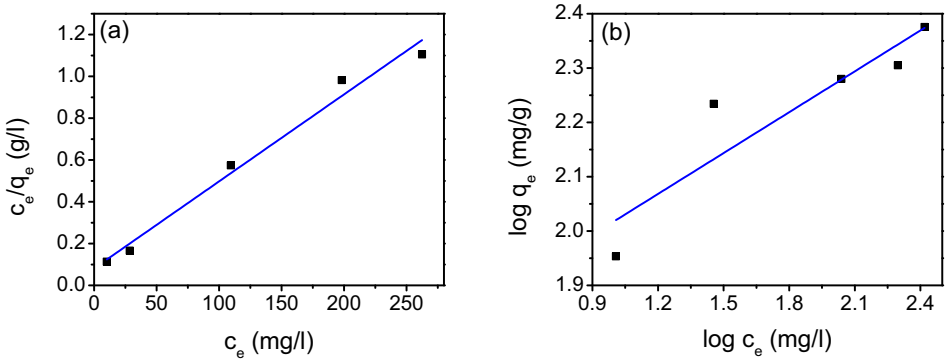

Fig. 7. The Langmuir (a) and the Freudlich (b) isotherm models applied for MB adsorption of the activated carbon. The fitting correlation coefficient for the Langmuir is better than that for the Freudlich.

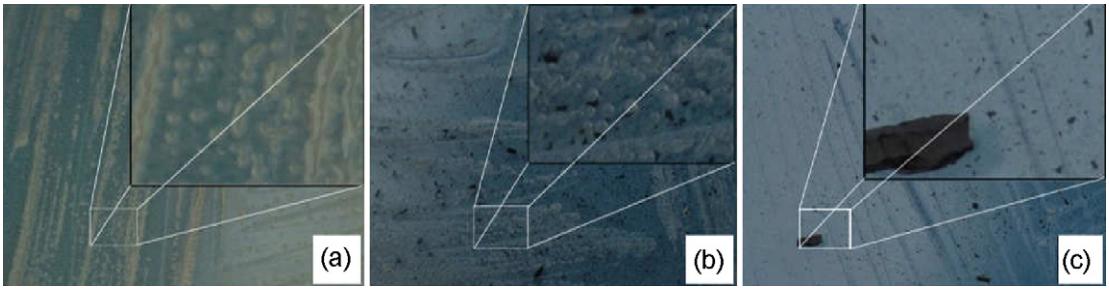

Fig. 8. Test samples for strains of *E. coli* in the agar dish for negative control (a), presence of AC (b) and presence of AgAC (c). The white colonies on figure (a) and (b) (see the insets for more detailed) show that the negative control allowed normal growth and AC did not inhibit the growth. No colony is observed in figure (c) confirming a strong inhibition against the growth of AgAC on *E. coli*.

tion by carbonized silver containing yeast cells and carbonized control yeast cells [50].

3.3. Antibacterial study

The qualitatively antibacterial study of AgAC on LB agar medium is shown in Fig. 8. Fig. 8(a) is the result in disk (a) for the negative control (Section 2.4) showing a normal growth of *E. coli* by the presence of white colonies on the agar plate (see the inset of the figure). Fig. 8(b) is the result for disk (b) presenting a normal growth of *E. coli* as well. This reveals that AC itself did not inhibit the growth of *E. coli*. Meanwhile in a parallel test, no *E. coli* colony can be observed in the agar plate in disk (c) (Fig. 8(c)). This result indicates that 0.15 g AgAC – equivalent to 1.5 mg AgNP provided a strong antibacterial activity against *E. coli*. The volume of LB agar medium in a Petri disk was 15 ml so that the concentration of AgNP in the Petri disk was 150 μg/ml. Our AgAC is a potential material for applications against microbial infection and contamination.

The quantitatively antibacterial study of AgNP in LB broth is shown in Fig. 9 which presents the dynamics of *E. coli* growth in LB broth for the negative control, TSC control and AgNP tests (AgNP concentration of 2—200 μg/ml). The initial number of *E. coli* inoculated in to 2 ml LB medium of the tested tube was 1.7×10^6 cells, providing the final bacterial concentration of 8.5×10^5 cells/ml. For the negative control and the TSC control, *E. coli* bacteria grew normally. The concentration of *E. coli* after 30 h in the TSC control ($OD_{595} = 2.5$) is higher than that in the negative control ($OD_{595} = 1.5$) which suggests that TSC was not toxic to *E. coli* and may be even enabled for the bacterial growth. The situation is different with the presence of AgNP because of the well-known antibacterial property of this metal [51]. When AgNP concentration was 2 μg/ml, the result is similar to the result of the negative control because the low value of AgNP could not inhibit bacteria growth. With higher AgNP concentration, the inhibitory effect occurred within 8 h even at low AgNP concentration of 4 μg/ml. This value is about 2-fold lower than the threshold concentration of 8 μg/ml reported for AgAC in another research [6] and slightly higher than a value of 2–3 μg/ml reported for the complicated Tollens process [52]. The minimal inhibitory concentration (MIC) is defined as the lowest concentration of a drug that will inhibit the visible growth of *E. coli* after a period of time long enough for the growth of single colony to a turbid bacteria culture observable by nake-eyes. Commonly it is overnight incubation. For longer incubation time, i.e., 24 and 30 h, *E. coli* grew in the broth tubes with AgNP concentration ≤12 μg/ml and inhibited in the broth tubes with AgNP concentration ≥16 μg/ml. Therefore the MIC of AgNP against the growth of *E. coli* is 16 μg/ml which is close to the MIC, normally ranging from 1 to 16 μg/ml, of antibiotics used for the treatment of *E. coli* [53]. The fact that no *E. coli* colony was observed in disk (c) of Fig. 8 is

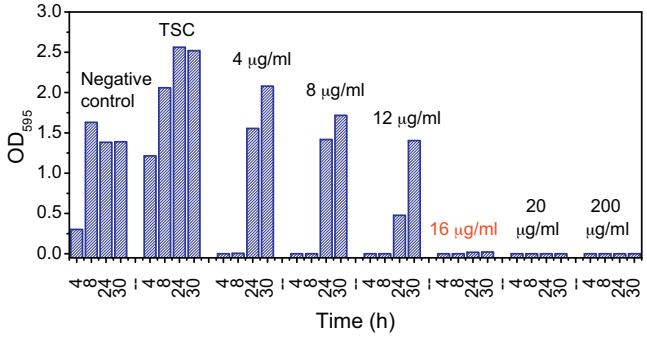

Fig. 9. Bar chart of OD_{595} reflecting *E. coli* concentration in LB in the presence of different concentrations of AgNP nanoparticles (μg/ml) as increasing time (h). Each test was conducted after 4, 8, 24 and 30 h. It is obvious that, with the concentration of AgNP ≥ 16 μg/ml, the *E. coli* growth was inhibited.

because the concentration of AgNP in AgAC (150 μg/ml) in the LB agar was nearly 10-fold higher than the MIC value of AgNP.

4. Conclusions

This paper presents a modified sonoelectrochemical technique which brings a versatile in choosing chemicals to obtain non-toxic nanosilver colloids. The principle of this technique can be applied to make other metallic nanoparticles. The antimicrobial activity of AgNP against *E. coli* was obtained at very low concentration with MIC value of 16 μg/ml. Silver nanoparticles were loaded in coconut-based AC prepared by thermal activation with water steam. The presence of AgNP did not change the surface property of the AC but improved As(V) adsorption. The significant inhibitory effect against bacteria of the material is expected to provide the end-user certain advantage in the prevention of foodborne illness, which is an alarming problem in developing and developed countries.

Acknowledgements

The study was financially supported by the key project QGTD.10.29 of Vietnam National University, Hanoi and the project 2/2010/HD-NCCBUD of Ministry of Science and Technology, Vietnam. The authors would like to thank Mr. Luu Manh Quynh for fruitful discussion and experimental helps.

References

[1] T.F. Clasen, D.H. Thao, S. Boisson, O. Shipin, Microbiological effectiveness and cost of boiling to disinfect drinking water in rural Vietnam, Environ. Sci. Technol. 42 (2008) 4255–4260.
[2] C. Flohr, L.N. Tuyen, S. Lewis, R. Quinnell, T.T. Minh, H.T. Liem, J. Campbell, D. Pritchard, T.T. Hien, J. Farrar, H. Williams, J. Britton, Poor sanitation and helminth infection protect against skin sensitization in vietnamese children: a cross-sectional study, J. Allergy Clin. Immunol. 118 (2006) 1305–1311.
[3] I.A.W. Tan, A.L. Ahmad, B. Hameed, Adsorption of basic dye on high-surface-area activated carbon prepared from coconut husk: Equilibrium, kinetic and thermodynamic studies, J. Hazard. Mater. 154 (2008) 337–346.
[4] L. Chan, W.H. Cheung, G. McKay, Adsorption of acid dyes by bamboo derived activated carbon, Desalination 218 (2008) 304–312.
[5] M. Kuroda, M. Yuzawa, Y. Sakakibara, M. Okamura, Methanogenic bacteria adhered to solid supports, Water Res. 22 (1988) 653–656.
[6] S. Pal, Y.K. Tak, J. Joardar, W. Kim, J.E. Lee, M.S. Han, J.M. Song, Nanocrystalline silver supported on activated carbon matrix from hydrosol: antibacterial mechanism under prolonged incubation conditions, J. Nanosci. Nanotechnol. 9 (2009) 2092–2103.
[7] I. Sondia, B. Salopek-Sondi, Silver nanoparticles as antimicrobial agent: a case study on *E. coli* as a model for gram-negative bacteria, J. Colloid Interface Sci. 275 (2004) 177.
[8] K.S. Lee, M.A. El-Sayed, Gold and silver nanoparticles in sensing and imaging: Sensitivity of plasmon response to size, shape, and metal composition, J. Phys. Chem. B 110 (2006) 19220.
[9] M. Ip, S.L. Lui, V.K.M. Poon, I. Lung, A. Burd, Antimicrobial activities of silver dressings: an in vitro comparison, J. Med. Microbiol. 55 (2006) 59–63.
[10] S. Pal, Y.K. Tak, J.M. Song, Does the antibacterial activity of silver nanoparticles depend on the shape of the nanoparticle? A study of the gram-negative bacterium Escherichia coli, Appl. Environ. Microbio. 73 (2007) 1712.
[11] J. Elechiguerra, J. Burt, J. Morones, A. Camacho-Bragado, X. Gao, H. Lara, M. Yacaman, Interaction of silver nanoparticles with HIV-1, J. Nanobiotechnol. 3 (2005) 6.
[12] V.K. Sharma, R.A. Yngard, Y. Lin, Silver nanoparticles: green synthesis and their antimicrobial activities, Adv. Colloid Interface Sci. 145 (2009) 83.
[13] S. Sedaghat, A. Nasseri, Synthesis and stabilization of ag nanoparticles on a polyamide (nylon 6,6) surface and its antibacterial effects, Int. Nano Lett. 1 (2011) 22–24.
[14] M.G. Guzman, J. Dille, S. Godet, Synthesis of silver nanoparticles by chemical reduction method and their antibacterial activity, Int. J. Chem. Bio. Eng. 2 (2009) 104–111.
[15] I. Lee, S.W. Han, K. Kim, Simultaneous preparation of SERS-active metal colloids and plates by laser ablation, J. Raman Spectrosc. 32 (2001) 947–952.
[16] D. Long, G. Wu, S. Chen, Preparation of oligochitosan stabilized silver nanoparticles by gamma irradiation, Radiat. Phys. Chem. 76 (2007) 1126–1131.
[17] K.A. Bogle, S.D. Dhole, V.N. Bhoraskar, Silver nanoparticles: synthesis and size control by electron irradiation, Nanotechnology 17 (2006) 3204–3208.
[18] H. Bonnemann, R.M. Richards, Nanoscopic metal particles—synthetic methods and potential applications, Eur. J. Inorg. Chem. 2001 (2001) 2455–2480.
[19] K. Mallick, M.J. Witcomb, M.S. Scurrell, Polymer stabilized silver nanoparticles: a photochemical synthesis route, J. Mater. Sci. 39 (2004) 4459–4463.
[20] H. Yin, T. Yamamoto, Y. Wada, S. Yanagida, Large-scale and size-controlled synthesis of silver nanoparticles under microwave irradiation, Mater. Chem. Phys. 83 (2004) 66–70.
[21] S. Navaladian, B. Viswanathan, R. Viswanath, T. Varadarajan, Thermal decomposition as route for silver nanoparticles, Nanoscale Res. Lett. 2 (2007) 44–48.
[22] J. Zhu, S. Liu, O. Palchik, Y. Koltypin, A. Gedanken, Shape-controlled synthesis of silver nanoparticles by pulse sonoelectrochemical methods, Langmuir 16 (2000) 6396–6399.
[23] A. Irzh, N. Perkas, A. Gedanken, Microwave-assisted coating of PMMA beads by silver nanoparticles, Langmuir 23 (2007) 9891–9897.
[24] O. Ioannidou, A. Zabaniotou, Agricultural residues as precursors for activated carbon production—a review, Renew. Sustainable Energy Rev. 11 (2007) 1966–2005.
[25] P.C. Lee, D. Meisel, Adsorption and surface-enhanced raman of dyes on silver and gold sols, J. Phys. Chem. 86 (1982) 3391–3395.
[26] N.H. Luong, N.N. Long, L.V. Vu, N.H. Hai, T.N. Phan, T.V.A. Nguyen, Metallic nanoparticles: synthesis, characterisation and application, Int. J. Nanotechnol. 8 (2011) 227–240.
[27] D. Kim, S. Jeong, J. Moon, Synthesis of silver nanoparticles using the polyol process and the influence of precursor injection, Nanotechnology 17 (2006) 4019–4024.
[28] H.H. Huang, X.P. Ni, G.L. Loy, C.H. Chew, K.L. Tan, F.C. Loh, J.F. Deng, G.Q. Xu, Photochemical formation of silver nanoparticles in poly(*N*-vinylpyrrolidone), Langmuir 12 (1996) 909–912.
[29] H.S. Shin, H.J. Yang, S.B. Kim, M.S. Lee, Mechanism of growth of colloidal silver nanoparticles stabilized by polyvinyl pyrrolidone in γ-irradiated silver nitrate solution, J. Colloid Interface Sci. 274 (2004) 89–94.
[30] V.I. Klimov (Ed.), Semiconductor and Metal Nanocrystals: Synthesis and Electronic and Optical Properties, Marcel Dekker, New York, 2004.
[31] R.A. Alvarez-Puebla, D.J. Ross, G.-A. Nazri, R.F. Aroca, Surface-enhanced Raman scattering on nanoshells with tunable surface plasmon resonance, Langmuir 21 (2005) 10504–10508.
[32] S. Link, M.A. El-Sayed, Shape and size dependence of radiative, non-radiative and photothermal properties of gold nanocrystals, Int. Rev. Phys. Chem. 19 (2000) 409–453.
[33] K.S.W. Sing, D.H. Everett, R.A.W. Haul, L. Moscou, R.A. Pierotti, R. Rouquerol, T. Siemieniewska, Reporting physisorption data for gas/solid systems with special reference to the determination of surface area and porosity, Pure Appl. Chem. 57 (1985) 603–619.
[34] N.H. Hai, I. Grigoriants, A. Gedanken, Converting Stöber silica and mediterranean sand to high surface area silicon by a reaction under autogenic pressure at elevated temperatures, J. Phys. Chem. C 113 (2009) 10521–10526.
[35] H.M.F. Freundlich, Over the adsorption in solution, Z. Phys. Chem. 57A (1906) 385–470.
[36] I. Langmuir, The constitution and fundamental properties of solids and liquids, J. Am. Chem. Soc. 38 (1916) 2221–2295.
[37] S. Lagergren, Zur theorie der sogenannten adsorption geloster stoffe, Kungliga Svenska Vetenskapsakademiens, Handlingar 24 (1898) 1–39.
[38] G. Blanchard, M. Maunaye, G. Martin, Removal of heavy metals from waters by means of natural zeolites, Water Res. 18 (1984) 1501–1507.
[39] C. Aharoni, D.L. Sparks, S. Levinson, I. Ravina, Kinetics of soil chemical reactions: relationships between empirical equations and diffusion models, Soil Sci. Soc. Am. J. 55 (1991) 1307–1312.
[40] B.H. Hameed, A.T.M. Din, A.L. Ahmad, Adsorption of methylene blue onto bamboo-based activated carbon: kinetics and equilibrium studies, J. Hazard. Mater. 141 (2007) 819–825.
[41] B.H. Hameed, R.R. Krishni, S.A. Sata, A novel agricultural waste adsorbent for the removal of cationic dye from aqueous solutions, J. Hazard. Mater. 162 (2009) 305–311.
[42] B.H. Hameed, M.I. El-Khaiary, Equilibrium, kinetics and mechanism of malachite green adsorption on activated carbon prepared from bamboo by K_2CO_3 activation and subsequent gasification with CO_2, J. Hazard. Mater. 157 (2008) 344–351.
[43] G. Crini, H. Peindy, F. Gimbert, C. Robert, Removal of c.i. basic green 4 (malachite green) from aqueous solutions by adsorption using cyclodextrinbased adsorbent: kinetic and equilibrium studies, Sep. Purif. Technol. 53 (2007) 97–110.
[44] R. Malik, D. Ramteke, S. Wate, Adsorption of malachite green on groundnut shell waste based powdered activated carbon, Waste Manage. 27 (2007) 1129–1138.
[45] C.A. Basar, Applicability of the various adsorption models of three dyes adsorption onto activated carbon prepared waste apricot, J. Hazard. Mater. 135 (2006) 232–241.
[46] I.D. Mall, V.C. Srivastava, N.K. Agarwal, I.M. Mishra, Adsorptive removal of malachite green dye from aqueous solution by bagasse fly ash and activated carbon-kinetic study and equilibrium isotherm analyses, Colloids Surf. A 264 (2005) 17–28.
[47] A.S. Alzaydien, Adsorption of methylene blue from aqueous solution onto a low-cost natural Jordanian tripoli, Am. J. Environ. Sci. 5 (2009) 197–208.
[48] Y. Liu, New insights into pseudo-second-order kinetic equation for adsorption, Colloids Surf., A 320 (2008) 275–278.
[49] D. Kavitha, C. Namasivayam, Experimental and kinetic studies on methylene blue adsorption by coir pith carbon, Bioresour. Technol. 98 (2007) 14–21.

[50] R. Selvakumar, N.A. Jothi, V. Jayavignesh, K. Karthikaiselvi, G.I. Antony, P. Sharmila, S. Kavitha, K. Swaminathan, As(V) removal using carbonized yeast cells containing silver nanoparticles, Water Res. 45 (2011) 583–592.
[51] J.S. Kim, E. Kuk, K.N. Yu, J.-H. Kim, S.J. Park, H.J. Lee, S.H. Kim, Y.K. Park, Y.H. Park, C.-Y. Hwang, Y.-K. Kim, Y.-S. Lee, D.H. Jeong, M.-H. Cho, Antimicrobial effects of silver nanoparticles, Nanomedicine 3 (2007) 95–100.
[52] L. Kvitek, A. Panacek, J. Soukupova, M. Kolar, R. Vecerova, R. Prucek, M. Holecova, R. Zboril, Effect of surfactants and polymers on stability and antibacterial activity of silver nanoparticles (NPS), J. Phys. Chem. C 112 (2008) 5825–5834.
[53] S. Kim, S.S. Kim, Y.J. Bang, S.J. Kim, B.J. Lee, In vitro activities of native and designed peptide antibiotics against drug sensitive and resistant tumor cell lines, Peptides 24 (2003) 945–953.